Walther et al. EPJ Techniques and Instrumentation (2015) 2:7
DOI 10.1140/epjti/s40485-015-0017-7

EPJ Techniques and Instrumentation
a SpringerOpen Journal

RESEARCH ARTICLE Open Access

An optimized measurement chamber for cantilever array measurements in liquid incorporating an automated sample handling system

Michael Walther, Paul M Fleming, Francesco Padovani and Martin Hegner*

* Correspondence: martin.hegner@tcd.ie
Centre for Research on Adaptive Nanostructures and Nanodevices (CRANN), School of Physics, Trinity College Dublin, Dublin 2, Ireland

Abstract

Micro- and nanomechanical analytical devices for diagnostics require small sample volumes, and stable and efficient clamping of the sensors for optimized bioassays. A fully automated device for the readout of the dynamic and static response of cantilevers in a physiological liquid environment including a sample handling system is presented. The device provides sequential readout of the static and dynamic mode providing the best signal to noise ratio for each individual cantilever. In the dynamic mode, it is possible to measure up to the 16th flexural resonance mode of vibration of a 500 μm long and 1 μm thick cantilever. The automated sample handling system enables the local injection of sub microliter volumes of sample with excellent reproducibility. Data demonstrating the response of the cantilevers to external stimuli highlight the sensitivity of the device and the importance of the use of reference cantilevers to decouple biologically relevant metrics from environmental effects. A specific biomolecular interaction of sensitised nanospheres on cantilever sensors with a mass resolution of ~50 picogram in liquid is shown.

PACS numbers: 07.10 Mechanical instruments, 87.85 Biosensors, 47.85. Fluidic

Keywords: Cantilever; Label-free sensing; Dynamic mode; Static mode; Fluidics; Micromechanical devices; Biosensor

Introduction

Cantilever technology has been used for a wide variety of applications including mass, force and biological sensing. Within the latter category, a large subset of sensing applications exists in the fields of proteomics [1-5], genomics [6-8] and microbiology [9-15], amongst others. A crucial component in achieving biologically relevant metrics in bio-sensing is the environment in which the test is performed. The mainstays in routine bio-sensing applications, such as ELISA and qPCR, are performed in physiological (liquid) environments. To bridge the gap between research and clinical laboratories, cantilever sensors must follow suit despite the challenges encountered when operating in fluid. Operating within a relevant biological environment affords considerable validity to the technique in comparison to a 'dip-dry' method [16].

The handling of liquid volumes takes on an increasing relevance when moving from a 'dip-dry' method to a continuous measurement format, as liquid is transferred to the

cantilever rather than the cantilever to the liquid. For efficient transfer of small volumes of liquids, the integration of micro-fluidic technologies, which already inevitably overlap with cantilevers in many fields, is desirable. Scaling down provides numerous advantages on both fronts; micro-cantilevers offer an increased sensitivity over their macro alternatives, and the conservation of precious samples in analytical techniques [17].

In order to de-couple environmental effects or spurious events from biologically relevant events, at least one reference cantilever should be used when utilising micro-cantilevers as bio-sensors [18]. These environmental effects can further exacerbate when working in a liquid environment in comparison to a micro-cantilever operated *in vacuo* and include temperature, viscosity, and liquid flow. Without the appropriate *in situ* reference cantilevers, a measured signal cannot confidently be attributed to the investigated analyte property only [16,19].

The device presented here incorporates a micro-cantilever array operated in both static and dynamic mode in a liquid environment. Arrays allow reference cantilevers to be designated and the elimination of environmental influences. Sub microliter sample volumes can be injected easily and the device can be operated in stop flow or in continuous flow mode. The read-out principle of the nanomechanical array is based on the optical beam deflection method [20]. The entire device is fully automated from optical alignment to sample injection, readout and analysis.

Device

The main components of the developed device consist of the fluidic chamber, the fluidics setup, the temperature control system and the optical beam deflection system. The fluidics chamber assembly, shown in Figure 1, contains elements for thermal monitoring, thermal control, piezoelectric actuation, injection of fluids and clamping of the cantilever array.

Fluidic chamber assembly

The chamber body is machined from Polyetherether-ketone (PEEK). The cantilever array is held within a recessed pocket which fixes the array at an angle of 18° to the glass cover (Figure 2). This angle is used in order to avoid the creation of any standing waves or internal reflections from the chamber walls that may cause additional frequency noise. The cantilever array is held firmly in place using a PEEK clamp screwed in place using two PEEK screws (Nippon Chemical Screw & Co., Ltd., Tokyo, Japan). This type of fixation stabilises the cantilever array and reduces drift after the introduction of fluid into the fluid chamber. Once the cantilever is fixed in place, a double anti-reflective coated glass cover (Schott AG, Mainz, Germany) is placed on top of a Viton® O-ring (Kubo Tech AG, Effretikon, Switzerland) or on top of a Nescofilm seal (Figure 3) and fixed in place using a black anodized aluminium frame. When the glass cover is fixed in place, the resulting fluid chamber volume is 4 μl.

The chamber body has two fluid inlets and two outlets. Extruded 1/16" Teflon tubing (Zeus, Orangeburg, USA) is connected at each flat-bottom port using M6 PEEK nuts and flangeless ferrules (Idex Corporation, Illinois, USA). The remaining port houses a micro-dispensing valve (The Lee Company, Connecticut, USA) fixed using a manifold mount such that the outlet nozzle is protruding directly into the flow stream. This

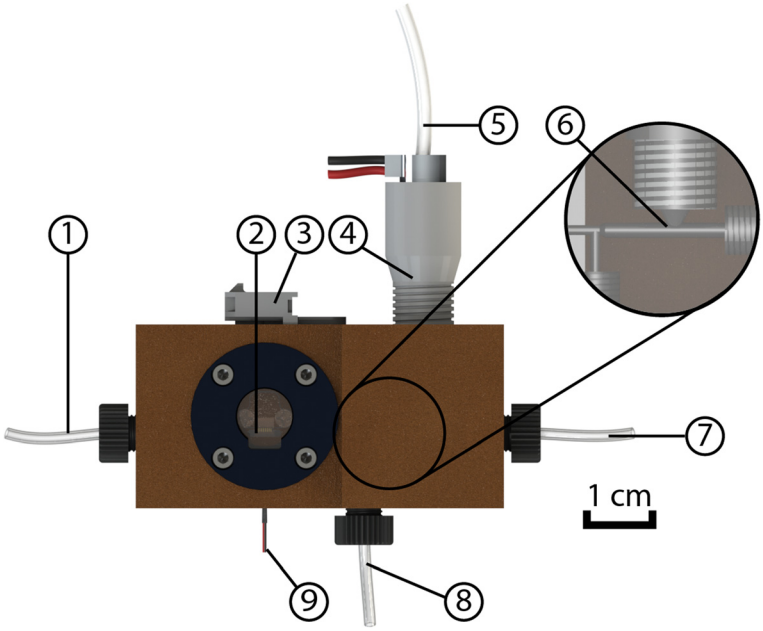

Figure 1 Fluidic chamber assembly. The inlet line (7) carries the buffer to the fluidic chamber. A sample line (5) connected to the sample reservoir (not shown) carries the sample fluid to the injection valve (6) where it is injected into the flow of the inlet buffer. The injection valve is held in place using a manifold mount (4). The fluid can then flow out through the priming line (8) or into the measurement chamber (2) depending on the orientation of the solenoid valve (not shown). A thermocouple (9) monitors the temperature inside the measurement chamber and the piezoelectric actuator connected at (3) can be used for dynamic mode operation. The outlet line (1) leads to a waste container.

configuration allows the implementation of additional inlet ports in a manifold configuration 'up-stream' of the first injection port without redesign of the core of the measurement chamber.

In order to obtain a wide range of resonance modes, a stack of piezoelectric actuators (EBL Products Inc., Connecticut, USA), assembled in-house with the size of the

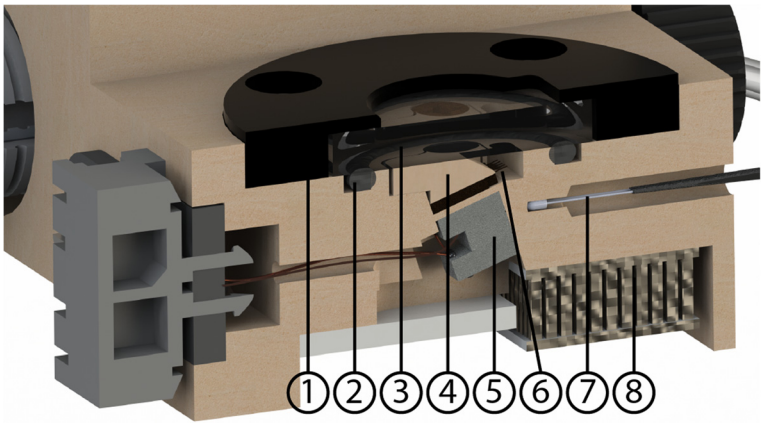

Figure 2 Chamber cross section. The cantilever array (6) is clamped in place using a PEEK clamp (4). An Oring (2) and the glass cover (3) allow the creation of a sealed measurement chamber. An aluminium clamp (1) holds the glass cover in place. A piezoelectric actuator (5) is fixed underneath the body of the cantilever array. A thermocouple (7) provides feedback on the measurement chamber temperature and a peltier element (8) allows the generation of a heat pulse.

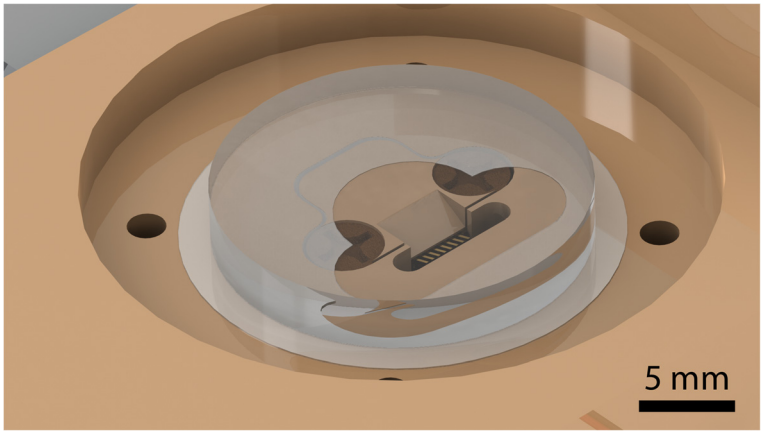

Figure 3 Close up of the Nescofilm used to seal the chamber instead of the o ring (aluminium clamp and screws not shown for clarity). The Nescofilm has a tickness of 90 μm and is placed underneath the glass cover.

cantilever array body, is mounted below the array body using TorrSeal® (Agilent Technologies Ltd., Torino, Italy). The stack is composed of three piezoelectric crystal layers each 1.0 mm thick. Two 2x3 mm^2 piezoelectric pieces (EBL Products INC., East Hartford, USA) and one 2x2 mm^2 piece (EBL Products INC., East Hartford, USA) are sandwiched together using electrically conductive epoxy resin (Epoxy Technology, Inc. Billerica, USA). The actuator is separated from the liquid chamber by a 200 μm thick PEEK membrane to prevent shorting. The membrane is sufficiently thin to allow adequate transfer of energy from the actuator to the cantilever (see Figure 2).

Adjacent to the piezoelectric actuator, and directly underneath the cantilever array, is situated a peltier module (Global Component Sourcing, Hong Kong). This module allows a heat pulse to be applied to the liquid chamber enabling a subsequent normalization of the nanomechanical response of the individual cantilevers to compensate for differences of their mechanical properties. A precision temperature sensor (Hygrosens Instruments GmbH, Löffingen, Germany) is placed in close proximity to the cantilevers in the PEEK chamber.

Fluidics

Liquid is introduced to the chamber using two different methods. A Genie™ Plus Syringe Pump (Kent Scientific Corporation, Connecticut, USA) is used to pump buffer through the chamber. The micro dispensing valve is used to introduce the sample of interest to the liquid line and is pressure driven. A compressed air regulator (Spectron Gas Control Systems GmbH, Frankfurt, Germany) provides the appropriate pressure in the 20 – 100 mbar regime and the desired volume is injected through controlling the opening time of the micro dispensing valve.

A three-way solenoid valve (ASCO Valve, Inc. Florham Park, NJ, USA) allows control over whether the liquid flows into the measurement chamber or whether it bypasses it using the priming outlet. The priming outlet is located between the measurement chamber and the two inlet ports. This outlet allows diverting bubbles and priming of the micro dispensing valve without introducing sample into the cantilever chamber before it is required.

Temperature control

Because the cantilever sensors are often coated on one side with one or more metal layers for subsequent chemical or biological functionalisation, care must be given to ensure a steady temperature. Fluctuations in temperature will result in the cantilever deflecting due to the difference in the thermal expansion coefficients of the silicon and the metal layers. Thermal fluctuations affect the viscosity and density of the liquid and therefore the oscillation frequency of the sensors. To ensure a steady temperature, the fluid chamber, the buffers, samples and peripheral equipment such as optics are all housed within a small refrigeration/heating unit (Intertronic, Interdiscount, Switzerland). A silent, vibration free fan (Zalman, Seoul, Korea) helped maintain a uniform temperature within the refrigeration unit.

Optical beam deflection system

Optical read-out is the most commonly used read out system and can give sub-angstrom resolution [18,20]. A single wavelength fibre-coupled laser diode (830 nm, 10 mW, C Pin Code, SM Fibre Pigtailed Laser Diode; LPS-830-FC; Thorlabs Ltd. Cambridgeshire, UK) was used. The laser has a free space power of 10 mW and a line width >200 kHz. Stabilisation within 1% is achieved once it has been turned on for 20 minutes. A combined laser diode and temperature controller (ITC4001 Benchtop Laser Diode/TEC Controller, 1 A/96 W; Thorlabs Ltd. Cambridgeshire, UK) allowed for a very stable output. The laser was coupled to a collimator (F260APC-780; Thorlabs Ltd. Cambridgeshire, UK) which collimated the beam to a 3.33 mm diameter. The laser beam is focused to a 14 μm spot on the cantilever using a 50 mm focal length achromatic doublet (AC127-050-B; Thorlabs Ltd. Cambridgeshire, UK).

The reflected laser spot is tracked using a linear position sensitive device (PSD 1 L10-10-A_SU15; SiTek Electro Optics AB, Partille, Sweden) with an in-house designed electric amplification circuit with a cut off at 2 MHz (3 dB), which extracts the differential and summation signal at a gain of 1. To avoid saturation of the PSD, a neutral density filter (NE506B-B; Thorlabs Ltd. Cambridgeshire, UK) can be inserted into the beam path to attenuate the laser.

Optical read-out of all eight cantilevers is possible by mounting the laser assembly within an optical cage system (Thorlabs Ltd. Cambridgeshire, UK) on high precision automated translation stages (122.2DD and M-110.1DG Precision Micro-Translation Stage; Physik Instrumente Ltd., Bedford, England). Aligning the stages to enable both x-axis and y-axis motion allows movement between cantilevers, and also adjustment to an optimum location along each cantilever. Particularly within dynamic mode operation, optimal amplitude signals can be obtained by individually positioning the laser on each cantilever separately, as this can compensate for subtle mechanical differences between the cantilevers. For the dynamic mode operation the laser has to be positioned and focussed on a flex point of the cantilever. For example, the node-to-node distance for the 16^{th} flexural resonance mode is ~33 μm, hence the angle sensitive region is approximately 11 μm long. The y-axis and x-axis miniature translation stages feature an optical linear encoder with 100 nm and 50 nm position resolution and a velocity of 20 mm/s and 1 mm/s respectively.

The precision automated translation stages are mounted on a three-axis translation stage (9061 Gothic-Arch XYZ Translation Stage, New Focus, Micro-Controle Spectra-Physics

S.A., Évry Cedex, France). The x-axis and y-axis stages both use manual micrometer heads (Mitutoyo; New Focus, Micro-Controle Spectra-Physics S.A., Évry Cedex, France). On the z-axis stage a picomotor actuator (Tiny picomotor actuator, Model 8353 Intelligent Picomotor driver; New Focus, Micro-Controle Spectra-Physics S.A., Évry Cedex, France) for automated positioning of the stage is implemented, hence facilitating automated positioning of the focal point of the achromatic lens on the cantilever surface. The z-axis actuator offers a resolution better than 30 nm with minimal backlash and a velocity of 0.016 mm/s. Moreover, it holds the position with no power applied resulting in a quick initialisation process. The path of the laser through the optical beam deflection system can be seen in Figure 4.

Operation

The device outlined can be operated in both dynamic and static mode. When set to dual mode operation, the laser spot cycles through the cantilevers sequentially, taking firstly a dynamic measurement and then a static measurement before moving onto the next cantilever. A LabVIEW (National Instruments, Texas, USA) program controls the movement of stages, dictates the frequencies sent to the piezoelectric actuator and performs analysis of the signals acquired by the PSD. LabVIEW is also used for temperature and fluidic control.

Automated laser focusing

To obtain the highest resolution possible for the static measurements, the laser has to be well focussed and positioned at the apex of the cantilevers where the maximum deflection occurs [21]. To acquire the maximum response for all the flexural modes of vibrations of a cantilever operated in dynamic mode, the laser has to be precisely positioned and focussed at a node of the cantilever [22]. Therefore, the widely used knife-edge technique [23-25] to determine the laser beam width is embedded in the LabVIEW code to perform the focusing of the laser on the cantilever automatically.

The laser is moved onto the cantilever where it is reflected onto the PSD. As the laser is then moved across the cantilever, the intensity of the reflected light is measured by

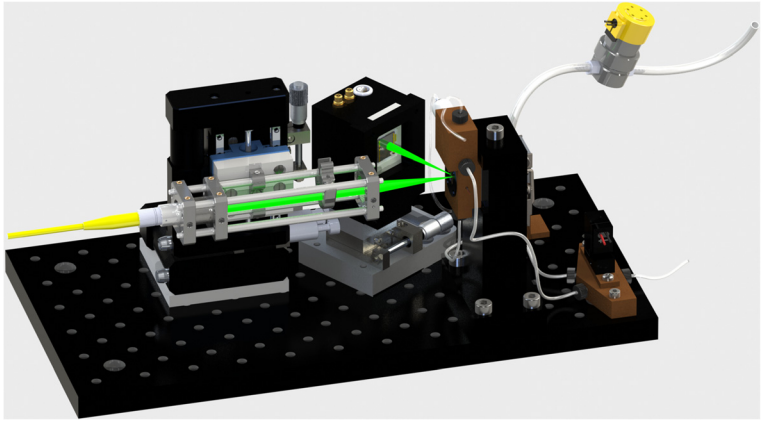

Figure 4 The path of the optical beam through the system is visually represented in green in this figure. The automated and manual translation stages, the laser and the focusing optics, the threeway solenoid valve and the PSD are all visible.

the PSD and recorded as a function of its position on the cantilever. By moving the laser off from the cantilever, less light is reflected and the measured sum signal continuously decreases to zero.

The revised Khosrofian and Garetz inversion algorithm [26] is used to calculate the radius of the laser beam where it hits the cantilever surface.

$$P_N(x) = \frac{1}{1 + exp[a_1 t + a_3 t^3]} \tag{1}$$

where $a_1 = -1.60$, $a_3 = -7.09 \times 10^{-2}$, $t = (2/w_x)(x - x_0)$, $P_N(x) = P(x)/P_T$ is the normalized power, w_x is the beam radius, x_0 is the initial position of the laser on the cantilever and x is the actual position on the cantilever.

The LabVIEW program iteratively changes the laser distance with respect to the cantilever and calculates the beam radius until a laser spot radius of less than 8 μm is achieved. This quick and inexpensive method gives an accurate determination of the laser spot radius, resulting in an optimally focused laser on the cantilever.

Dynamic mode measurement

When operating in dynamic mode, the stages move the laser spot to a previously set location along each cantilever. A frequency generation board (NI PCI 5406; National Instruments, Texas, USA) outputs a frequency sweep to the piezoelectric actuator such that the cantilevers are excited at selected frequency bandwidths. The PSD differential output is pre-amplified with low power high-speed operational amplifiers (LT1358CS8 Linear Technology, Milpitas, CA, USA) before final amplification with a low-noise preamplifier (SR560; Stanford Research Systems, California, USA) and then digitised (NI PCI 5112; National Instruments, Texas, USA). The optimal range of the 8-bit digitiser can be precisely set to the achieved voltage signal after the amplification (120 different ranges are selectable via NI SCOPE software). The signal is then analysed in LabVIEW, which presents amplitude and phase frequency spectra, an example spectrum is shown in Figure 5. All raw data is output to a text file. For each spectrum (e.g. scanning two peaks), 3000 data points are measured per peak with a sampling rate of 5×10^6 samples/s. Each data point is the average of 5×10^3 samples.

Static mode measurement

When operating in static mode, the stages move the laser spot to a location close to the tip of the cantilever. After pre-amplification, the output from the PSD is input to a data acquisition board (NI PCI 6221, National Instruments, Texas, USA). The movement of the laser along the cantilevers allows the extraction of the curvature of the sensors [22,27]. The mean differential and sum signals are then used in the LabVIEW program to calculate the deflection of the cantilever using the formula [28],

$$x = \frac{I_1 - I_2}{I_1 + I_2} \frac{L}{2} G \tag{2}$$

where $(I_1\text{-}I_2)$ is the differential signal from the PSD, (I_1+I_2) is the sum signal from the PSD, L is the length of the PSD and G is the calibration factor specific for each setup obtained by geometrical calculation [29] or by a thermal method [30]. The differential and sum signals are sampled at a rate of 10^5 samples/s and each data point is the average of 2500 samples.

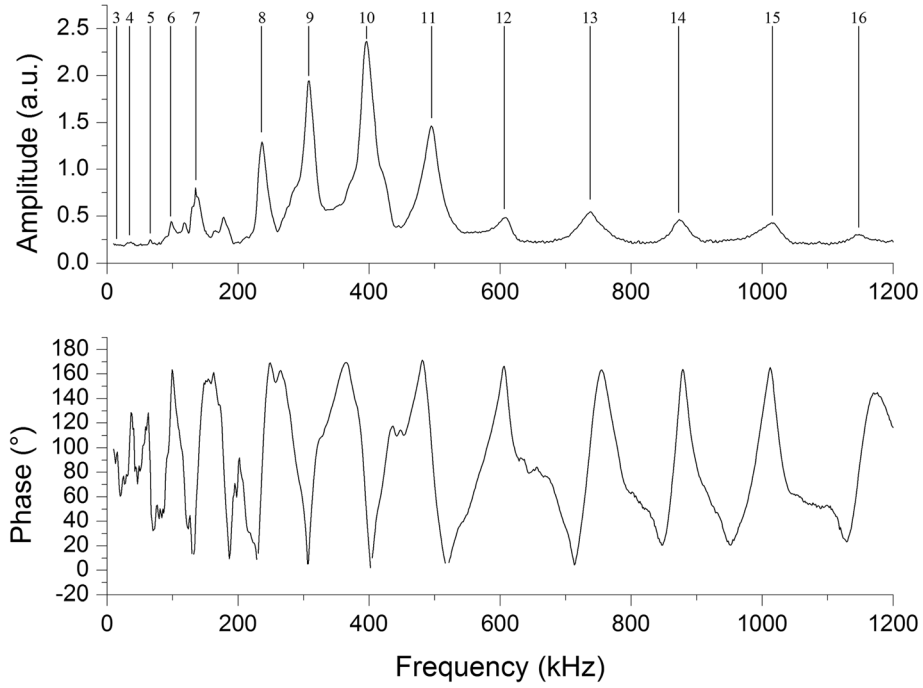

Figure 5 Amplitude and phase spectra of a 1 μm thick, 500 μm long cantilever from the arrays used in the measurement chamber. Flexural resonance modes from 3 to 16 are clearly visible in the frequency range up to 1200 kHz [33].

Experimental

Cantilever Arrays

Silicon cantilever arrays (IBM Research Laboratory, Rüschlikon, Switzerland) with eight cantilevers per array were used for all measurements. The cantilevers had a thickness of 1 μm, a length of 500 μm and a width of 100 μm. The cantilevers were designed with a 250 μm pitch and cantilevers from the same wafer possessing the same dimensions were used for all experiments.

Automated laser focusing

The laser was moved onto the initial position on the cantilever where it was reflected onto the PSD. As the laser was then moved across the cantilever, the intensity of the reflected light was measured by the PSD and recorded as a function of its position on the cantilever. The model from De Araújo [26] was fitted to the experimental data and the radius of the laser beam on the cantilever surface was obtained. Based on the obtained radius, the optical cage was moved closer or further away from the measurement chamber followed by the next measurement to obtain the radius of the newly focused laser beam. This process was repeated until the laser was finely focused on the cantilever. The depth of focus of the laser of several tens of microns allowed for variation in the position along the x-axis without compromising the focussing of the laser.

Thermal noise versus active dynamic actuation with the integrated piezo

A cantilever array was loaded into the fluid chamber and allowed to equilibrate in deionized water. For the thermal noise power spectrum of the sensors a frequency

domain from 0 - 18 kHz was analysed with a sampling rate of 90 kHz and a frequency resolution of 0.1 Hz. The parameters for the power spectrum analysis were: a Hamming window [31] with 200 rms averages. The data can be further smoothed without loosing data information applying a Savitzky-Golay algorithm [32]. Within this range the first, second and third harmonic of the 1 μm thick cantilevers in liquid could be investigated. The voltage signal of the differential thermal noise on the PSD could be amplified by factors up to 5000 without driving the sensors with the integrated piezo-electric stack. Alternatively the sensors were then actively driven with the piezo-electric stack by applying an actuation voltage within the range of 2 – 5 volts through the software.

Temperature effects

A cantilever array was loaded into the fluid chamber and allowed to equilibrate in nanopure water. When the temperature reached steady state at 23.1°C, dual mode measurement was started. Every two hours, the set-point temperature was increased by 0.5°C until a temperature of 24.1°C was reached. The temperature stability at the set point is ±0.02°C.

The dual mode sweep occurred every 30 seconds, upon which dynamic mode measurements, static mode deflection and temperature were recorded. For the dynamic mode operation, the range for the frequency sweep was set from 200 kHz to 500 kHz within which three resonance mode peaks were contained [33]. To ensure that only bimetallic effects of the sensors contribute to the evaluated static cantilever signal a chip with solid sidebars in position 0 and 9 was scanned. These additional signals showed that the drift of the device is neglectable [34].

Flow rate effects

A cantilever array was loaded into the fluid chamber and allowed to equilibrate in nanopure water. When the temperature reached steady state at 23°C, dual mode measurement was started. The flow rate was set to 2 μl/min, 5 μl/min, 10 μl/min, 25 μl/min, 50 μl/min and 100 μl/min sequentially for 30 minutes each. The buffer reservoir was within the temperature controlled unit to ensure a uniform temperature throughout the experiment.

The dual mode sweep occurred every 30 seconds, upon which dynamic mode measurements and temperature were recorded. For the dynamic mode operation, the range for the frequency sweep was set from 250 kHz to 400 kHz within which two resonant mode peaks were contained.

Sealing of the Chamber

The influence of O-ring or Nescofilm sealing on the static mode signal was investigated. A cantilever array was loaded into the fluid chamber that was subsequently sealed either with Nescofilm or an O-ring and allowed to equilibrate in nanopure water. After equilibration, the static mode measurement was started. Nanopure water was introduced into the chamber at a flow rate of 10 μl/min for 45 minutes or in a second experiment 2 μl/min for 5 minutes.

Volume of injected samples

A 100 μl volume of nanopure water was loaded into the sample reservoir and the injection valve was primed. A series of injections at a constant pressure of 100 mbar were

performed with increasing valve opening times from 31 ms to 40 ms in 1 ms increments. The sample injection line was secured along a graduated surface and the sample meniscus was monitored after each injection to determine the volume of fluid injected. A digital microscope (Dino-Lite Pro HR AM7000 series; Dino-Lite, The Netherlands) was used to give the required resolution. To determine the volume injected, the pixel location of the meniscus along the graduated scale was determined using images from before and after injection. This pixel differential was then converted to length, and hence volume (ranging from 4 to 5 μl), using the ratio of millimetres to pixels which could be easily calculated using image analysis software.

A series of ten 500 nl samples were also injected to investigate the reproducibility of the injected volumes and were analysed using the same method as above.

Viscosity effects

A cantilever array was loaded into the measurement chamber and allowed to equilibrate in 5% glycerol solution (v/v). When the temperature reached steady state at 23°C, dual mode measurement was started. After 15 minutes, a 10 μl volume of 12% ethylene glycol (v/v) was injected, which is enough to exchange the liquid in the fluid chamber. After a further 30 minutes, the measurement chamber was flushed with 100 μl of 5% glycerol solution at a flow rate of 20 μl/min. The 5% glycerol solution has a theoretical viscosity of 1.055 cP while the 12% ethylene glycol's viscosity is 1.257 cP at 20°C.

The sweep occurred every 15 seconds, upon which dynamic mode measurement and temperature were recorded. For the dynamic mode operation, a frequency sweep between 250 kHz and 600 kHz was generated within which three resonance mode peaks were tracked.

A viscosity change from water (1.0 cP at 20°C) to 12% ethylene glycol (v/v) (1.257 cP at 20°C) was induced to analyse the benefit from an actively versus thermal noise driven system. For comparison the same viscosity change from water to ethylene glycol solution at mode 13 was investigated. The thermal noise peaks were fitted using a Lorentzian fit to enhance the visibility of the resonance peaks and to determine the resonance frequency.

Density effects

A cantilever array was loaded into the measurement chamber and allowed to equilibrate in 5% glycerol solution (v/v). When the temperature reached steady state at 23°C, dynamic mode measurement was started. After 15 minutes, a 10 μl volume of 5% ethylene glycol (v/v) was injected. After a further 30 minutes, the measurement chamber was flushed with 100 μl of 5% glycerol solution at a flow rate of 20 μl/min. The 5% glycerol solution has a theoretical density of 1010 kg/m^3 while the 5% ethylene glycol's density is 1003 kg/m^3 at 20°C.

The sweep occurred every 15 seconds, upon which dynamic mode measurement and temperature were recorded. For the dynamic mode operation, a frequency sweep between 200 kHz and 550 kHz was generated within which three resonance-mode peaks were tracked.

Biological assay

To compare the performance of the new fluidics and measurement chamber to previous experiments a biomolecular recognition proof of concept experiment for biological

sensing was implemented. A chip with 8 gold coated sensors was functionalised with ω-terminated alkyl-thiols to form self-assembled monolayers [35]. Four sensors were functionalised with a hydroxy-terminated functional group (H338, Dojindo, Munich, Germany) and four with a biotin-terminated group (B564, Dojindo, Munich, Germany) in a 1 mM concentrated ethanol solution in a micro-capillary functionalisation tool [7] for 30 minutes at room temperature. After the functionalisation the sensors were thoroughly rinsed with first ethanol, water and then with PBS buffer (pH 7.4).

As a target for biomolecular specific interactions polystyrene spheres (diameter 810 nm, 3.42 x 10^{10} beads/ml, SVP-08-10 Spherotech, Lake Forest, IL) functionalised with streptavidin were utilised. 10 μl of beads were washed by re-suspending the sedimented pellet three times with 1 ml PBS after centrifugation for 5 minutes at 5000 rpm. Finally the beads were resuspended at a concentration of 3.42 × 10^8 beads per μl.

After initial equilibration of the sensors in PBS buffer with 10 μl/min flow at 24°C for five minutes the buffer was stopped for 13 minutes. During this wait time the sample volume of 10 μl streptavidin beads was loaded upstream of the measurement chamber with the micro-dispensing valve into the liquid channel by opening the priming channel. Then the sample was pushed into the liquid chamber with a speed of 10 μl/min for two minutes to ensure full exchange. The flow was then stopped for 10 minutes to facilitate a specific interaction of the streptavidin spheres with the biotin – or hydroxyl functionalised sensors. To conclude the experiment the chamber was rinsed for 20 minutes with PBS buffer at 10 μl/min. During the whole biological assay two resonance peaks per sensor (mode 10 and 11) with 3000 data points per peak were measured with a sampling rate of 5 × 10^6 samples/s. Each data point is the average of 5x10^3 samples. To plot the data, the signals of four biotinylated and four of the hydroxyl functionalised cantilevers were individually averaged. The frequency shifts measured were converted to mass changes using the formulas given in ref [36].

Results and Discussion

Automated laser focusing

Figure 6 shows the experimental data of the final step of the laser focusing process and a fitting of the experimental data with equation I. The obtained laser beam radius was 7.177 μm. This quick method of the laser focusing gave an accurate determination of the laser spot radius, hence an optimally focused laser on the cantilever for the static and dynamic mode measurements.

Thermal — versus active dynamic actuation

In order to assess the sensitivity and noise within the micromechanical sensor experiment, thermal noise power spectra of the cantilever arrays in liquid with a bandwidth of 0 - 18 kHz were recorded and analysed. We investigated the effect of signal amplification and active actuation of the cantilevers with the integrated piezo-electric stack. As shown previously in [22,37] the piezo-stack mounted underneath the cantilever sensor array can be oscillated to drive the cantilever motion. The amplitude response of the piezo within the frequency domain of interest is nonlinear, providing higher excitation responses at higher frequencies [22]. In Figures 7 and 8 we demonstrate the beneficial effect of the active actuation of cantilever sensors in order to enhance higher

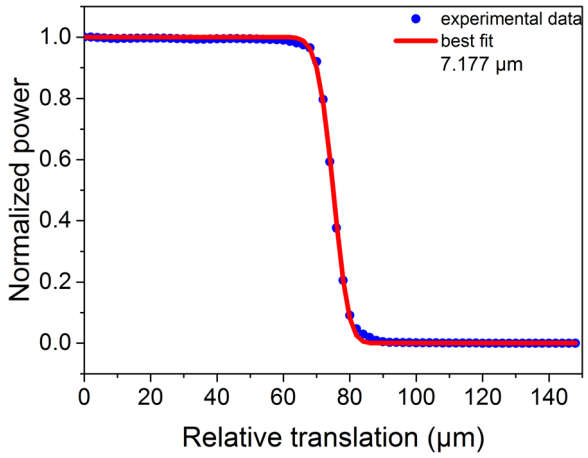

Figure 6 Measured normalized reflected power of the laser beam by the PSD as a function of the laser position in the x direction on the cantilever. By fitting equation (I) to the data a laser beam radius of 7.177 μm was obtained.

order oscillation peaks. A cantilever structure was oscillating at its natural frequency driven by thermal noise, this feature can also be used to calibrate the cantilever spring constant [38] and to gain the G-factor of the device [30]. The cantilevers chosen in these experiments with a thickness of 1 μm and a length of 500 μm exhibited a natural frequency 1st mode at 620 Hz, 2nd mode at 5.15 kHz and 3rd mode at 16.1 kHz. The signals generated by the PSD electronics (I/V converter) without amplification were in the μV range. For an optimal electronic read-out they needed to be boosted into the

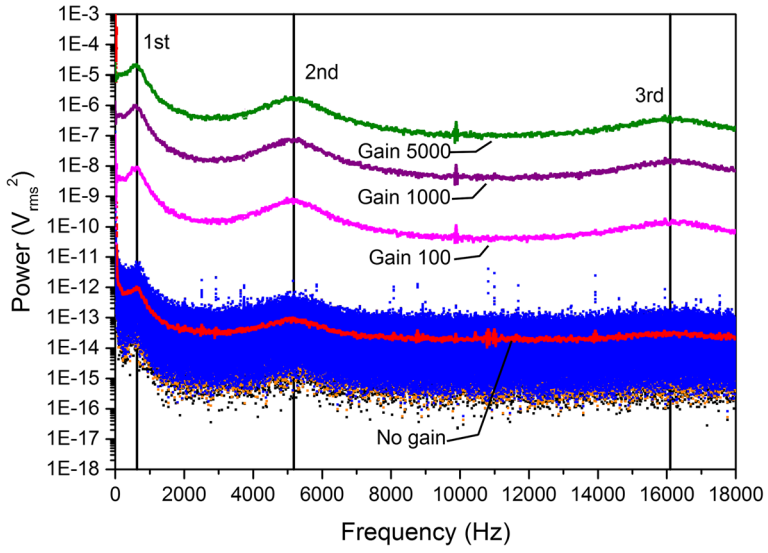

Figure 7 Thermal noise versus signal amplification. The thermal noise spectrum signal of the eight individual sensors is plotted from 0 – 18 kHz. The individual spectra were overlaid and were matching each other (the signal of the eighth sensor (blue) is masking the other individuals underneath). Applying the Savitzki-Golay filter allowed clearer extraction of the frequency information (in red) and to remove high frequency noise [32]. Signal amplification using the Stanford instruments SR560 digitisers ranged up to 5000 fold. The vertical input range of the boosted signal was then precisely set with the 8-bit digitizer board. No additional spectral features appeared within the log scale in the y-axis.

mV to volt range. In order to assess whether the low-noise pre-amplifier was distorting the initial frequency response the signal was amplified. As seen in Figure 7, the quality of the natural resonance peaks remained preserved within the range of gain up to 5000 fold. We plotted the thermal noise spectrum of all the eight sensors also without any gain. The mechanical properties of the sensors were congruent and the individual resonance frequencies were within <0.5% range. This aspect is important for proper differential read-out analysis, only sensors with equal mechanical properties should be utilized for differential readout.

In Figure 8 we report on the quality of the micromechanical resonance spectra of the cantilevers within the array applying an actuation voltage on the piezo-electric stack mounted underneath the cantilever array. The frequency response of the piezo-electric stack was non-linear and showed an increased performance towards higher frequencies [22]. By driving the piezo-electric stack up to 4 - 5 volts we generated optimal detectable resonance peaks at higher modes. The actuation settings normally used for data acquisition were around ± 4 volts (range ± 0 - 5 volts) and a gain of 500. The resonance peaks at higher modes could be easily visualised (up to mode 16 in this publication) whereas in a situation when only thermal 'noise' would be used, natural frequencies higher than mode 2 would not be recognisable. The differential signal contribution for specifically measured interactions that change the mass of the sensors scale proportionally with higher modes. Therefore the implementation of a piezo-electric stack with the size of the cantilever array mounted directly underneath the sensor chip was highly beneficial to boost the sensitivity of the method [39].

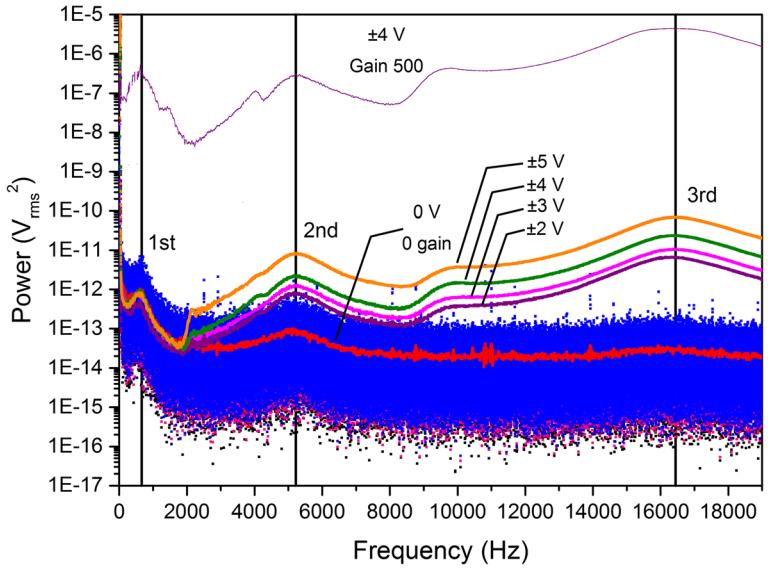

Figure 8 Actively driven cantilever array. The actuation of the piezo-electric stack that was mounted directly underneath the cantilever chip allowed boosting individual sensor frequency responses. The piezo-electric stack exhibits a non-linear response towards higher frequencies. Resonance oscillation peaks were amplified which was enhancing their detectability. Actuation voltages from 2 - 5 volts are shown, the response was non linear and the y-axis is displayed in a log scale. For routine measurements an actuation voltage around 4 volts with a gain of 500 was chosen.

Temperature

Static and dynamic mode measurements for an individual cantilever are shown in Figure 9 along with the corresponding temperature recorded through time. Corresponding jumps in the static and frequency signals are clearly visible as the temperature was increased. This highlights the sensitivity of the micromechanical method to temperature changes in static and dynamic mode. In layered structures such as silicon cantilevers coated with noble metals due to the different thermal expansion coefficients of the silicon and the 2 nm titanium and 21 nm gold layer deposited on the upper surface of the cantilevers (Si: 2.6×10^{-6} K^{-1}, Ti: $8.6 \times 10^{-6}K^{-1}$ and Au: $14 \times 10^{-6}K^{-1}$) temperature effects are significant and have to be considered at all times. In dynamic mode, the shift observed in resonance frequency was due to the changing properties of the cantilever and the surrounding liquid (most likely by the change in viscosity) with a change in temperature. At an increased temperature, the density and viscosity of the liquid decreased resulting in less co-moved mass by the

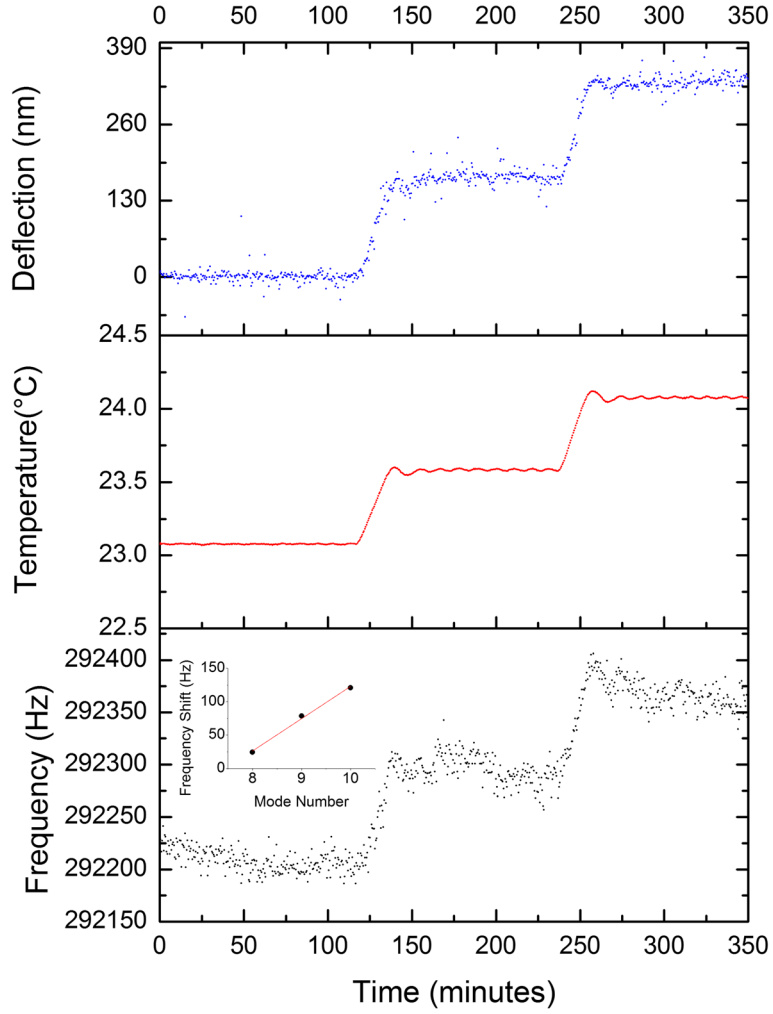

Figure 9 Static and dynamic response of the cantilever to increases in temperature. The dynamic response of the 9th flexural resonance mode and static response of the cantilever could be seen to closely track any changes in temperature over time. Here, two 0.5°C increases in temperature resulted in ~170 nm deflections in static mode (noise ±15 nm) and frequency shifts of ~75 Hz in dynamic mode (noise ±20 Hz). The insert shows the averaged absolute frequency shift of the tracked flexural resonance modes 8, 9 and 10. The errors of the averaged frequency shifts were as large as the symbols.

cantilever, hence the resonance frequency increased. The flexural resonance mode 9 was analysed. As a control to investigate the overall drift of the measuring chamber made from PEEK (thermal expansion coefficient PEEK: 50×10^{-6} K^{-1}) the signal of a solid side bar [34] was analysed in parallel. The overall drift of the static signal of solid side bar, equivalent to the drift in the device, for a temperature change of 1°C was within the measurement error of ± 2 nm (data not shown). The inset of Figure 9 shows the average frequency shift for mode 8, 9 and 10 due to a temperature increase of 0.5°C. The sensitivity was a linear function of mode number indicating that higher modes were more susceptible.

To highlight the importance of differential measurements using reference cantilevers, Figure 10 shows a plot of the dynamic signal of two cantilevers at the 13th higher mode at ca. 724 kHz responding to temperature and the differential signal between both cantilevers. The differential signal showed the elimination of these environmental effects using a reference cantilever, considering a homogeneous mixing in the fluid chamber and no temperature gradient within the chamber. A single cantilever taken on its own would show a significant change in resonance frequency (indicating a viscosity change) of 225 Hz whereas the differential signal was 0 ± 30 Hz.

Flow rate

Figure 11 shows a plot of the centre frequencies of two resonance peaks plotted against time for a range of increasing flow rates. It was observable that there was no frequency shift as the flow rate increased, nor was there any effect in the noise of the system. The peak-to-peak noise level of the raw data for mode 9 was ~140 Hz and for mode 10 ~300 Hz. Additionally, the filtered raw data is shown. This makes the dynamic mode, in particular, also suitable for use in continuous flow experiments.

Sealing of the chamber

Figure 12 shows the average static responses of the all the cantilevers per array to the flow of liquid at a rate of 10 μl/min for 45 minutes through the chamber sealed with

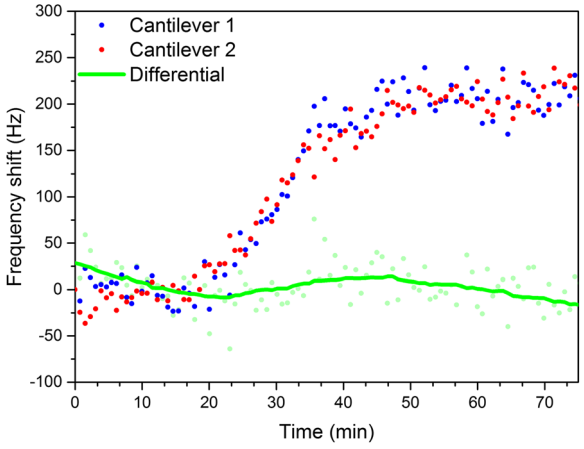

Figure 10 Differential dynamic mode signal. The plots of cantilevers 1 and 2 showed the change in resonance frequency of 225 Hz of mode 13 (noise ±30 Hz) of the cantilevers due to an increase in temperature by 0.5°C. However, the differential signal (green) showed how environmental effects such as temperature could be reduced through using a reference cantilever, as the differential signal was 0 ± 30 Hz.

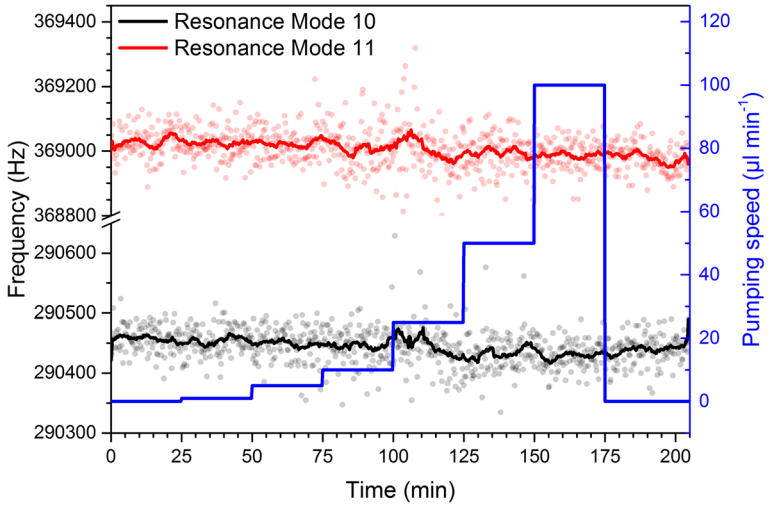

Figure 11 Flow rate effects. Two resonance modes plotted against time for a variety of flow rates showed little change in their frequencies as the flowrate was increased. The peak to peak noise level of the raw data for mode 9 and 10 was ~140 Hz and ~300 Hz, respectively.

either the Nescofilm or the O-ring. The sealing introduced an elastic element to the chamber that induced minimal displacements of the glass cover. These displacements could affect quality of the optical read-out of the cantilever responses. Considering utilising the differential read-out method eliminated such flow-induced features completely. Comparing the two sealing methods showed that the read-out of the Nescofilm seal was less affected by the elastic element, resulting in a more stable signal.

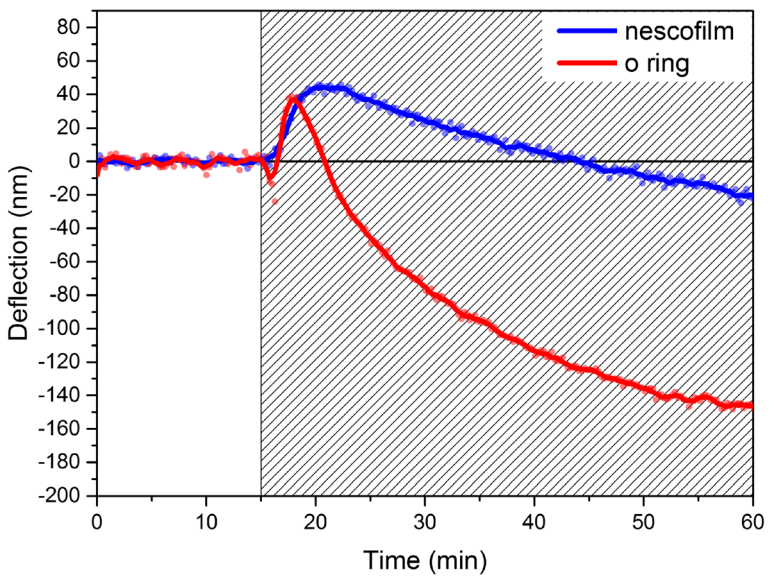

Figure 12 Average static response of all the cantilevers per array to the flow of liquid at a rate of 10 µl/min (hatched section) through the chamber sealed with either the Nescofilm (blue data) or the O-ring (red). The optical read-out of the cantilever response was less affected by the less elastic sealing method using the Nescofilm than using the O-ring. Both methods were applicable for the experiments, as long the sensors within an array responded in the same way to flow. By applying a differential read-out such flow induced signals were eliminated.

Figure 13 shows the individual static response of 6 cantilevers to the insertion of 10 μl liquid with a flow rate of 2 μl/min (hatched section). Pulling or pushing the liquid through the chamber resulted in a comparable response of the sensors (data not shown). The individual static mode data of the cantilevers featured a noise of ±3-5 nm. The selected flow rate together with the minimal required amount of liquid are key for a maximal stable signal of the sensors.

Volume of injected samples

Figure 14A shows a plot of sample volume against valve opening time and clearly highlighted how adjusting the opening time of the valve could control the volume injected. Here volumes from 4 μl to 5 μl could be injected by varying the opening time by 10 ms at 100 mbar with an initial sample volume in the reservoir of 80 μl. If finer control of the injected volumes is required, then the reservoir pressure can also be adjusted.

While Figure 14A shows slight variation around the trend line, it does not give an indication of the reproducibility of the injection volume using set parameters. A series of ten 500 nl volumes (at 100 mbar) were injected and their volume plotted against droplet number (shown in Figure 14B). Excellent reproducibility was demonstrated as the coefficient of variation (CV) for this series of droplets was 1.3%. A video highlighting the injection and exchange of the solution in the measurement compartment is shown in (Additional file 1).

Viscosity

Figure 15 shows the flexural resonance frequencies of modes 9, 10 and 11 of one cantilever and further demonstrates the sensitivity of the cantilevers to changes in its immediate environment. A stable frequency was recorded when a 5% glycerol solution (1.055 cP) was static in the measurement chamber. After the injection of a 10 μl volume of 12%

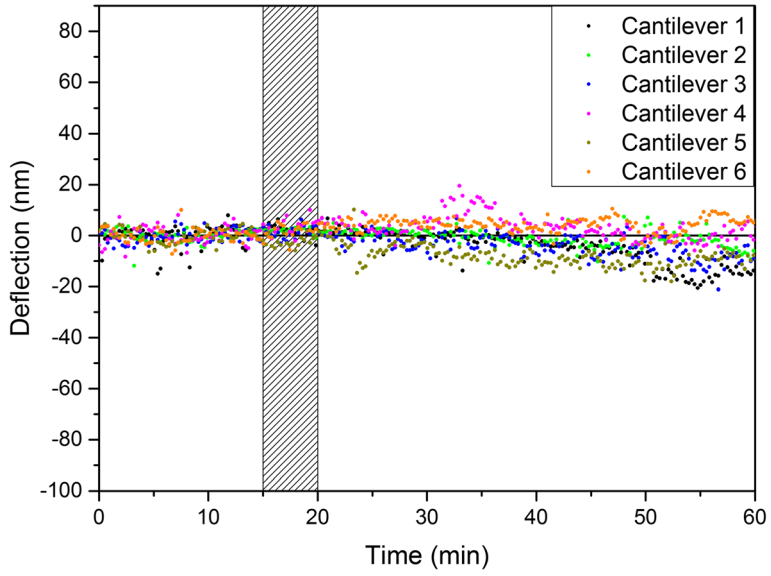

Figure 13 This plot shows the individual static response of 6 cantilevers to the insertion of 10 μl liquid with a flow rate of 2 μl/min (hatched section). This setting guarantied a full exchange of the liquid in the chamber and offered a maximal stability of the sensors (noise level of ~3-5 nm for each cantilever).

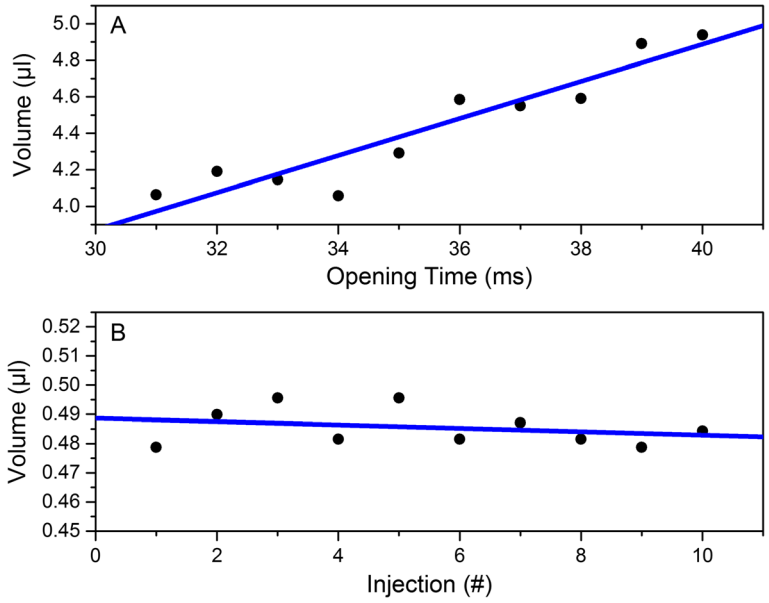

Figure 14 Precision sample dosage. **A)** This plot shows the dependence of the injected volume on the opening time of the injection valve. Droplets between 4 µl and 5 µl could be created by varying the opening time from 31 ms to 40 ms. **B)** A plot showing the reproducibility of a series of 500 nl injections into the chamber. A coefficient of variation of 1.3% highlighted the excellent reproducibility of the injections.

ethylene glycol solution (1.257 cP), a frequency decrease of ~385 Hz for mode 9, ~575 Hz (mode 10) and ~810 Hz (mode 11) could be observed. Upon flushing the measurement chamber again with the 5% glycerol solution, the frequency could be seen to recover to its previous stable value. This highlights the sensitivity of higher modes of the cantilever array to changes in viscosity in its surroundings with constant density.

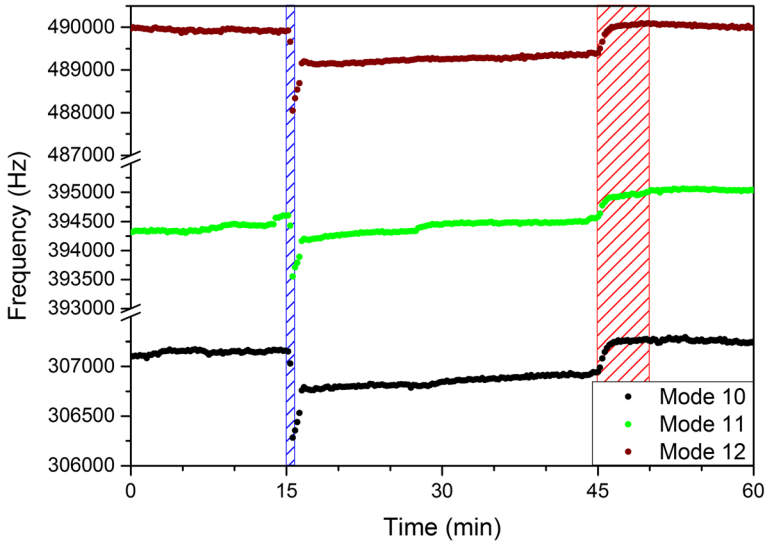

Figure 15 Viscosity effects. A stop flow experiment highlighting the effects of viscosity on frequency. A stable frequency was measured initially for 5% glycerol solution before the injection of a 10 µl volume of 12% ethylene glycol (injection took place in the hatched blue section). The frequency shifted towards lower frequencies for all modes (mode 9 by ~385 Hz, mode 10 by ~575 Hz and mode 11 by ~810 Hz) due to the increased viscosity. The frequency recovered to its previous values after flushing with 100 µl of 5% glycerol solution (hatched red section).

In Figure 16 the scaling of the sensitivity by applying higher resonance modes was demonstrated. The 1st resonance peak of the cantilevers in water was oscillating at 542 Hz whereas the same mode in ethylene glycol vibrated at 538 Hz. This shift of 4 Hz was barely visible considering the thermal noise of the measurement. The second mode showed a shift of ~170 Hz from 5068 Hz down to 4916 Hz, also here the noise within the measurement was affecting the analysis. In the inset we show the same viscosity change measured at the 13th mode ~688 kHz, when the liquid was changed to 12% ethylene glycol the frequency shifted by 4 kHz and was easily detected. Here actuating the piezo-stack with ± 4 volts and amplifying the signal with a gain of 500, as in other experiments, enhanced the oscillation and the subsequent analysis. Furthermore according to the simple harmonic oscillator model the acquisition time in the first modes (e.g. 640 Hz) has to be considerably longer than in higher modes (e.g. mode 10 at 395 kHz), by factor up to 25x, in order to let the cantilevers reach the steady state condition [40].

Density

Figure 17 shows the effect of changing fluid density on the 9th flexural resonance mode of the cantilevers. A stable frequency was recorded when the 5% glycerol solution (1010 kg/m^3) was static in the measurement chamber. After the injection of a 10 μl volume of 5% ethylene glycol solution (1003 kg/m^3), a ~115 Hz frequency shift could be observed for all cantilever shown. Upon flushing the measurement chamber with the 5% glycerol solution, the frequency could be seen to recover to its previous stable values. The increase in resonance frequency was due to the decrease in density and hence the reduction in virtual mass moved by the cantilever.

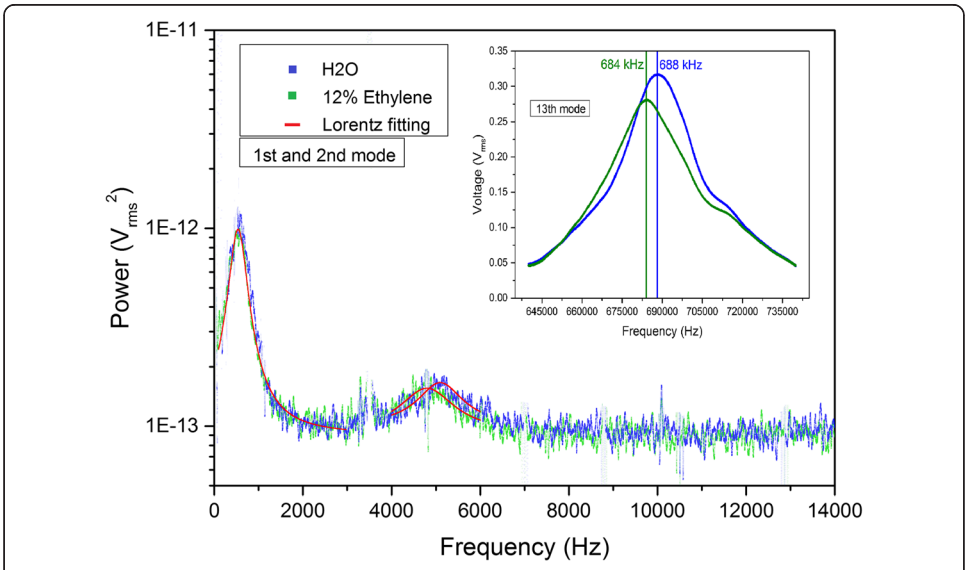

Figure 16 Viscosity effects. Thermal noise spectrum of 0 – 18 kHz is shown. The natural frequencies were shifting upon increasing the viscosity of the solution surrounding the cantilevers. The first mode shifted by 4 Hz whereas the second mode shifted by 170 Hz. The shifts could only be estimated when the signals were fitted with a Lorentzian function and remained elusive. Measuring at a higher mode e.g. mode 13, (the shift for the same viscosity change by 0.257 cP) resulted in a frequency shift of 4 kHz. The frequency noise in the measurements shown was in the order of 10 Hz.

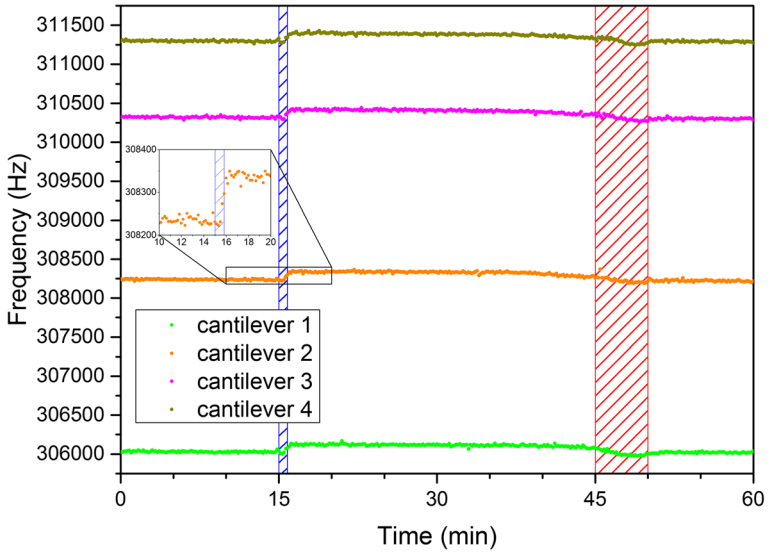

Figure 17 Density effects. A stop flow experiment highlighting the effects of density on frequency. Modes 9 of 4 cantilevers are shown. A stable frequency was measured initially for 5% glycerol solution before the injection of a 10 μl volume of 5% ethylene glycol (injection in the hatched blue section). The frequencies shifted by ~115 Hz in all sensors due to the decreased density of the solution and hence a lower virtual mass moved by the cantilevers (inset). The frequencies recovered to their previous values after flushing with 50 μl of 5% glycerol solution (hatched red section).

Biological assay

A biological assay was introduced to compare the results obtained with the new optimised measurement chamber to previous results where mass changes upon biological interaction were evaluated [36,3,11,39,37,5,22,16,15,12,21]. The response of four sensors functionalised with biotin-terminated self-assembled monolayers, a ligand interacting firmly with the protein receptor streptavidin, was utilized. To enhance the mass load the streptavidin was covalently coupled to polystyrene spheres with an average diameter of 810 nm and an individual mass of ~ 280 fg. In Figure 18A the raw data of the frequency evolution of the eight micromechanical sensors is shown, whereas in 18B the differential mass-load after subtraction of the changes in the reference sensors is presented. After an initial equilibration of the functionalised cantilever array in a PBS buffer solution at pH 7.4 a 10 μl volume containing 3.42×10^8/μl streptavidin beads was injected into the measurement chamber and the solution stopped for 10 minutes. During this time the beads could diffuse freely within the measurement chamber containing the sensitised cantilever array. As an *in situ* control four cantilevers were functionalised with a hydroxyl terminated self-assembled monolayer, which normally repels biological interactions. Since the cantilevers were only functionalised with gold on one side of the sensor, to enable static mode measurements, the sidewalls and the backside of the sensors remained uncovered and exposed bare silicon. After a rinse of the sensors with PBS buffer at a speed of 10 μl/min the frequency shifts were evaluated. Both sets of cantilevers, the biotin- and the hydroxy-functionalised ones, experienced a frequency decrease indicating a binding of the streptavidin spheres. The specifically functionalised biotin sensors showed a frequency decrease of ~270 Hz (*i.e.* ~1.29 ng), a larger shift of 40 Hz (180 pg) than the *in-situ* reference levers that shifted only by ~230 Hz (~1.11 ng) in the 10^{th} vibrational mode. The frequency

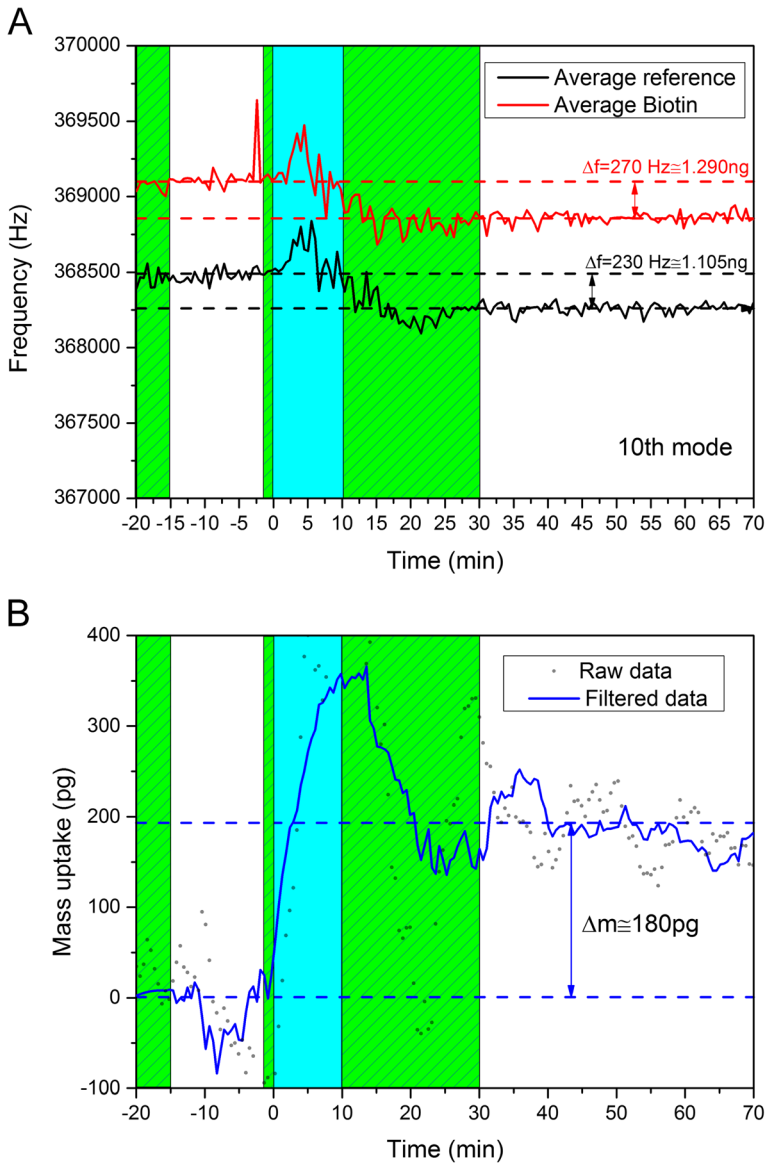

Figure 18 Specific biomolecular recognition of streptavidin functionalised polystyrene spheres with biotinylated cantilever sensors. Green hatched areas depict flow of liquids at 10 μl/min. **A)** Frequency response of the cantilever arrays. The response of four biotin functionalised sensors was averaged and the response of the four hydroxyl functionalised sensors that act as an *in situ* reference was averaged as well. At t = -2 min 10 μl containing 3.42x 10^8/μl of beads were injected for two minutes, this ensured the complete mixing/exchange of the beads in the measurement chamber. During the subsequent 10 minutes the cantilevers were exposed to the beads (light blue area) without flow. Beads were diffusing and were binding onto the sensors. After a fast initial mass uptake at 45 pg/min the curve was showing saturation with a reduced speed of ~10 pg/min. The biotinylated sensors experienced a differential frequency shift of 540 Hz. At t = 10 min the solution of the beads was rinsed out of the measurement chamber for 20 minutes and the flow stopped again. During rinsing unspecifically bound beads dissociated and the measured frequency shift corresponded to 270 Hz on the biotinylated sensors whereas on the hydroxyl functionalised sensor the reduction in frequency measured 230 Hz. **B)** Differential readout of specific mass uptake of the streptavidin functionalised spheres. The raw data is shown as dots in the background, the data filtered with the Savitzki–Golay filter shown as a continuous line. Data for all the eight sensors in liquid at the tenth higher oscillation mode were continuously recorded. The data acquisition for all eight sensors took 50 seconds, then the next measurement point was added. Due to the differential analysis data acquired during flow was noisier than data measured in phases where the flow was stopped.

noise in these measurements was in the range of 10 Hz corresponding to a differential mass noise of approximately 50 pg. This represented a increase in sensitivity of a factor 10 compared to the initial measurements in 2005 [36]. It is important to note that both sensors picked up mass during the experiment. With the *in situ* reference unspecific contributions to the changes in mechanical parameters e.g. streptavidin beads binding to the silicon surface of the backside of the sensors can be eliminated in real-time. In Figure 18B the specific mass uptake is presented. The mass noise was in the order of 50 pg. During the flow and incubation of the sensors in PBS buffer only, no significant changes could be observed. Upon injection of the 3.42×10^9 streptavidin beads (810 nm diameter) and their incubation in the chamber with the flow stopped, the mass was rapidly increasing and started to saturate after 10 minutes. During this phase of the experiment the frequency response was noisier due to laser scattering. After rinsing the beads out of the chamber it was noticed that about half of the added mass was lost, but could be attributed to streptavidin spheres that might have been bound in clusters without interacting with biotin on the sensor surface due to molecular recognition. After the rinse the differential signal started to equilibrate at a value of ~180 pg of gained mass. With a polystyrene density of 1.05 g/cm^3 this mass change amounted to 640 beads bound specifically to the biotinylated sensor interface covering 0.6% of the sensor surface. If the same experiment had performed at the first oscillation mode at 640 Hz, the shift in the frequency would correspond to 60 mHz requiring a frequency resolution of 15 mHz (in Figure 16 the frequency resolution is at 100 mHz). The small volume of the liquid system and the chamber enables minute injections within minutes and the optimised actuation and read-out of the sensor higher mode response allows precise evaluation of specific events happening at the interface.

Conclusion

A completely automated device for readout of the dynamic and static response of cantilevers in a physiological environment is presented. The device enabled the local injection of sub microliter volumes of sample with excellent repeatability. Reducing the sample volume from previously hundreds of μl [22,41] to a few μl enables the ability to generate larger volumes of data from the same total sample volume and hence the conservation of precious samples. We investigated the effect of the chamber seal on the nanomechanical measurement with either a thin membrane or a conventional O-ring. Both sealing methods are valuable for all liquid experiments and create a 4 μl measurement chamber which requires approximately 10 μl of liquid for full exchange. A slow injection speed (2 μl/min) is recommended in static mode measurements to minimise hydrodynamic bending of the sensors. The complete automation of the device including laser focusing allows the greatest resolution possible from experiment to experiment and reduces error due to user interactions. A series of experiments demonstrating the response of the cantilevers to external stimuli (temperature, viscosity, density, flow rate) highlight the sensitivity of the device. The difficulty of deconvoluting unambiguously relevant biological events in measurements using a single nanomechanical sensor is highlighted when one considers any sample introduced to the sensor may have a slight variation in temperature/viscosity/refractive index to the buffer fluid. It also serves to emphasise the importance of the use of *in situ* reference cantilevers to decouple biologically

relevant metrics from environmental effects in real-time as shown when cantilevers are used as specific biosensors.

Additional file

Additional file 1: Movie of liquid exchange in cantilever array measurement chamber. The exchange of liquids in the measurement chamber as observed with video microscopy. To exchange the complete liquid volume of the chamber a volume of 10 µl and an injection speed of 10 µl/min was chosen. After one minute the color of the liquid within the chamber is changed to a full intensive orange color (food dye) demonstrating exchange of the liquid. To rinse the chamber a pumping speed of 50 µl/min is chosen. After 100 µl respectively two minutes the chamber volume again appears completely transparent.

Competing interests
The authors are named as inventors in a patent application covering the measurement chamber.

Authors' contributions
MH and MW conceived and designed the experiments. MW re-designed the optimized cantilever array measurement chamber, PF incorporated the automatic sample handling system. MW, PF and FP performed the experiments. All authors analyzed and discussed the results and co-wrote the paper. All authors read and approved the final manuscript.

Acknowledgements
This work was supported by Science Foundation Ireland under the CSETscheme SFI08/CE/I1432, PI scheme SFI/09IN/1B2623 and SFI12/TIDA/B2380.

Received: 17 November 2014 Accepted: 27 April 2015
Published online: 12 May 2015

References
1. Arntz Y, Seelig JD, Lang HP, Zhang J, Hunziker P, Ramseyer JP, et al. Label-free protein assay based on a nanomechanical cantilever array. Nanotechnology. 2003;14(1):86–90.
2. Backmann N, Zahnd C, Huber F, Bietsch A, Plückthun A, Lang H-P, et al. A label-free immunosensor array using single-chain antibody fragments. Proc Natl Acad Sci U S A. 2005;102(41):14587–92.
3. Braun T, Ghatkesar MK, Backmann N, Grange W, Boulanger P, Letellier L, et al. Quantitative time-resolved measurement of membrane protein–ligand interactions using microcantilever array sensors. Nat Nanotechnol. 2009;4(3):179–85.
4. Waggoner PS, Varshney M, Craighead HG. Detection of prostate specific antigen with nanomechanical resonators. Lab Chip. 2009;9(21):3095–9.
5. Jensen J, Farina M, Zuccheri G, Grange W, Hegner M. Quantitative. Label-Free Detection of the Aggregation of α-Synuclein Using Microcantilever Arrays Operated in a Liquid Environment Journal of Sensors. 2012;2012:8740861–7.
6. Fritz J, Baller MK, Lang HP, Rothuizen H, Vettiger P, Meyer E, et al. Translating biomolecular recognition into nanomechanics. Science. 2000;288(5464):316–8.
7. McKendry R, Zhang J, Arntz Y, Strunz T, Hegner M, Lang HP, et al. Multiple label-free biodetection and quantitative DNA-binding assays on a nanomechanical cantilever array. Proc Natl Acad Sci U S A. 2002;99(15):9783–8.
8. Mertens J, Rogero C, Calleja M, Ramos D, Martín-Gago JA, Briones C, et al. Label-free detection of DNA hybridization based on hydration-induced tension in nucleic acid films. Nat Nanotechnol. 2008;3(5):301–7.
9. Ilic B, Czaplewski D, Craighead HG, Neuzil P, Campagnolo C, Batt C. Mechanical resonant immunospecific biological detector. Appl Phys Lett. 2000;77(3):450–2.
10. Ilic B, Yang Y, Craighead HG. Virus detection using nanoelectromechanical devices. Appl Phys Lett. 2004;85(13):2604–6.
11. Gfeller KY, Nugaeva N, Hegner M. Micromechanical oscillators as rapid biosensor for the detection of active growth of *Escherichia coli*. Biosensors Bioelectron. 2005;21(3):528–33.
12. Nugaeva N, Gfeller KY, Backmann N, Lang HP, Düggelin M, Hegner M. Micromechanical cantilever array sensors for selective fungal immobilization and fast growth detection. Biosensors Bioelectron. 2005;21(6):849–56.
13. Ramos D, Tamayo J, Mertens J, Calleja M, Villanueva LG, Zaballos A. Detection of bacteria based on the thermomechanical noise of a nanomechanical resonator: origin of the response and detection limits. Nanotechnology. 2008;19(3):035503.
14. Maloney N, Lukacs G, Nugaeva N, Grange W, Ramseyer JP, Jensen J, et al. Fibre optic readout of microcantilever arrays for fast microorganism growth detection. Journal of Sensors. 2012;2011:4052811–6.
15. Maloney N, Lukacs G, Jensen J, Hegner M. Nanomechanical sensors for single microbial cell growth monitoring. Nanoscale. 2014;6:8242–9.
16. Johnson BN, Mutharasan R. Biosensing using dynamic-mode cantilever sensors: A review. Biosensors Bioelectron . 2012;32(1):1–18.
17. Nguyen N-T, Wereley ST. Microfluidics for Life Sciences and Chemistry. Fundamentals and applications of microfluidics. Boston: Artech House; 2002. p. 373-452.
18. Boisen A, Dohn S, Keller SS, Schmid S, Tenje M. Cantilever-like micromechanical sensors. Rep Prog Phys. 2011;74(3):036101–31.
19. Longo G, Alonso Sarduy L, Rio LM, A. B, Trampuz A, J. N et al. Rapid detection of bacterial resistance to antibiotics using AFM cantilevers as nanomechanical sensors. Nature Nanotech. 2013;8(7):522-6.
20. Meyer G, Amer NM. Simultaneous measurement of lateral and normal forces with an optical-beam-deflection atomic force microscope. Appl Phys Lett. 1990;57(20):2089–91.

21. Tamayo J, Pini V, Kosaka P, Martinez NF, Ahumada O, Calleja M. Imaging the surface stress and vibration modes of a microcantilever by laser beam deflection microscopy. Nanotechnology. 2012;23(31):315501–9.
22. Jensen J, Maloney N, Hegner M. A multi-mode platform for cantilever arrays operated in liquid. Sensors Actuators B Chem. 2013;183:388–94.
23. Arnaud JA, Hubbard WM, Mandeville GD, de la Clavière B, Franke EA, Franke JM. Technique for fast measurement of gaussian laser beam parameters. Appl Opt. 1971;10(12):2775–6.
24. Khosrofian JM, Garetz BA. Measurement of a Gaussian laser beam diameter through the direct inversion of knife-edge data. Appl Opt. 1983;22(21):3406–10.
25. Bachmann L, Zezell MD, Maldonado PE. Determination of beam width and quality for pulsed lasers using the knife-edge method. Instrumentation Science & Technology. 2003;31(1):47–52.
26. de Araújo MA, Silva R, de Lima E, Pereira DP, de Oliveira PC. Measurement of Gaussian laser beam radius using the knife-edge technique: improvement on data analysis. Appl Opt. 2009;48(2):393–6.
27. Mertens J, Álvarez M, Tamayo J. Real-time profile of microcantilevers for sensing applications. Appl Phys Lett. 2005;87(23):234102.
28. Anssi M. Position-sensitive devices and sensor systems for optical tracking and displacement sensing applications. Academic Dissertation, Faculty of Technology, University of Oulu, Finland. 2000.
29. Miyatani T, Fujihira M. Calibration of surface stress measurements with atomic force microscopy. J Appl Phys. 1997;81(11):7099–115.
30. Mishra R, Grange W, Hegner M. Rapid and reliable calibration of laser beam deflection system for microcantilever-based sensor setups. Journal of Sensors. 2012;2011:6173861–6.
31. Hamming R. Numerical methods for scientists and engineers. New York: McGraw-Hill; 1962.
32. Savitzky A, Golay MJE. Smoothing and differentiation of data by simplified least squares procedures. Anal Chem. 1964;36(8):1627–39.
33. Van Eysden CA, Sader JE. Frequency response of cantilever beams immersed in viscous fluids with applications to the atomic force microscope: Arbitrary mode order. J Appl Phys. 2007;101:044908.
34. Huber F, Lang HP, Hegner M, Despont M, Drechsler U, Gerber C. Analyzing refractive index changes and differential bending in microcantilever. Rev Sci Instrum. 2008;79(8):086110.
35. Love JC, Estroff LA, Kriebel JK, Nuzzo RG, Whitesides GM. Self-assembled monolayers of thiolates on metals as a form of nanotechnology. Chem Rev. 2005;105:1103–69.
36. Braun T, Barwich V, Ghatkesar MK, Bredekamp AH, Gerber C, Hegner M. Mass sensors for biomolecular detection in physiological environment. Phys Rev E. 2005;72(031907):1–9.
37. Ghatkesar MK, Braun T, Barwich V, Ramseyer JP, Gerber C, Hegner M, et al. Resonating modes of vibrating microcantilevers in liquid. Appl Phys Lett. 2008;92(4):043106.
38. Hutter JL, Bechhoefer J. Calibration of atomic-force microscope tips. Rev Sci Instrum. 1993;64:1868–73.
39. Ghatkesar MK, Barwich V, Braun T, Ramseyer JP, Gerber C, Hegner M. Higher modes of vibration increase mass sensitivity in nanomechanical microcantilevers. Nanotechnology. 2007;18:445502.
40. Bhushan B. Nanotribology And Nanomechanics: An Introduction. Springer (India) Pvt. Limited; 2008.
41. Mishra R, Hegner M. Effect of non-specific species competition from total RNA on the static mode hybridization response of nanomechanical assays of oligonucleotides. Nanotechnology. 2014;25(22):225501.